Colloids and Surfaces B: Biointerfaces 171 (2018) 123–133

Contents lists available at ScienceDirect

Colloids and Surfaces B: Biointerfaces

journal homepage: www.elsevier.com/locate/colsurfb

Beta-carotene-bound albumin nanoparticles modified with chlorin e6 for breast tumor ablation based on photodynamic therapy

Pham Thi Thu Phuong[a], Sungin Lee[a], Changkyu Lee[a], Bohyung Seo[a], Sanghyun Park[a], Kyung Taek Oh[b], Eun Seong Lee[c], Han-Gon Choi[d], Beom Soo Shin[a,*,1], Yu Seok Youn[a,*,1]

[a] School of Pharmacy, Sungkyunkwan University, 2066 Seobu-ro, Jangan-gu, Suwon, Gyeonggi-do, 16419, Republic of Korea
[b] College of Pharmacy, Chung-Ang University, 221 Heukseok dong, Dongjak-gu, Seoul 06974, Republic of Korea
[c] Division of Biotechnology, The Catholic University of Korea, 43-1 Yeokgok 2-dong, Wonmi-gu, Bucheon-si, Gyeonggi-do 14662, Republic of Korea
[d] College of Pharmacy, Hanyang University, 55, Hanyangdaehak-ro, Sangnok-gu, Ansan 15588, Republic of Korea

ARTICLE INFO

Keywords:
Beta-carotene
Photodynamic therapy
Chlorin e6
Nanoparticles
Albumin
Tumor targeting

ABSTRACT

Chlorin e6 (Ce6) has attracted considerable interest as a promising second-generation photosensitizer for photodynamic therapy (PDT). However, the *in vivo* availability of Ce6 is significantly restricted by its low water solubility and poor ability to target tumors. We sought to overcome the limitations of Ce6 by using albumin nanoparticles with nab™ (nanoparticle albumin-bound) technology. The fabricated albumin nanoparticles consisted of bovine serum albumin (BSA), Ce6-BSA, and beta-carotene as a carrier, photosensitizing agent, and cross-linker, respectively. These albumin nanoparticles (Ce6-BSA-BC-NPs) did not include any toxic chemotherapeutics but instead contained naturally safe beta-carotene and Ce6, which was activated only upon irradiation with 660-nm laser light. Ce6-BSA-BC-NPs were ~120 nm in size and spherical, similar to Abraxane®, and showed good physicochemical stability. The nanoparticles showed significant cytotoxicity toward 4T1 cells as evaluated by MTT, Live/Dead, and TUNEL assays. In particular, results of the TUNEL assay demonstrated that cell death induced by Ce6-BSA-BC-NPs and light irradiation (660 nm) occurred through the apoptotic pathway. Ce6-BSA-BC-NPs displayed a remarkably enhanced tumor suppression effect when irradiated by 660-nm light compared with free Ce6 (tumor volume 90 ± 39 versus 487 ± 69 mm^3 respectively). Overall, this improved *in vivo* antitumor efficacy seemed to be due to the targetability of albumin nanoparticles. We believe that our Ce6-BSA-BC-NPs with PDT offer a promising new potential therapeutic platform for breast cancer treatment.

1. Introduction

Photodynamic therapy (PDT) has been considered an effective means of ablating tumors. The process of PDT involves administration of a tumor-localizing photosensitizer (PS) and timely local irradiation of tumor regions using light appropriate for the PS [1,2] Under appropriate levels of tissue oxygen and intensity of light the PS generates reactive oxygen species (ROS) such as singlet oxygen or free radicals [3], which induce cancer cell death through apoptosis, necrosis or autophagy [1,4,5]. Three mechanisms of tumor ablation by PDT have been suggested: (i) direct tumor cell killing, (ii) damage to tumor vasculature, and (iii) tumor suppression via the immune response [3]. PDT shows many advantages such as alleviated invasiveness, short treatment time, safety even after repetition, minimal scarring after healing, and low cost compared with other treatments [1,6,7]. PDT has been tested clinically for the treatment of various cancer types including head and neck, brain, lung, pancreas, skin, prostate and breast cancer [3].

Chlorin e6 (Ce6) is one of the most outstanding PSs developed to date and its derivatives have been used clinically for PDT. Compared with the first-generation PS, Ce6 responds to a greater range of wavelengths, between 600 and ~900 nm, which enables higher penetration of laser light into deep tissues. Furthermore, it shows strong intrinsic fluorescence over the wavelength range and can be effectively applied for diagnostic imaging of tumors without interference from endogenous chromophores [8]. However, the availability of Ce6 is restricted by its poor water solubility and low targetability.

Efficient localization of PS in tumors is essential for successful PDT because the amount of PS in tumors is directly related to the efficiency of ROS generation upon irradiation. Many studies have used the tumor

* Corresponding authors.
E-mail addresses: bsshin@skku.edu (B.S. Shin), ysyoun@skku.edu (Y.S. Youn).
[1] These authors equally contributed to this work.

https://doi.org/10.1016/j.colsurfb.2018.07.016
Received 6 April 2018; Received in revised form 5 June 2018; Accepted 9 July 2018
Available online 10 July 2018
0927-7765/

targetability of nanoparticles to address the limited availability of PSs in tumors for PDT. Among a number of nanoparticle platforms, albumin nanoparticles have attracted considerable interest in both academia and industry due to noticeable advantages of albumin protein as a pharmaceutical carrier, such as, biodegradability, biocompatibility, non-immunogenicity (human source), high chemical stability, and versatility. [9–11]. Moreover, albumin preferentially accumulates in tumor tissues due to its excellent targetability to tumors. It permeates leaky blood vessels via efficient extravasation process [12] and is transported across endothelial walls around tumor tissues through gp60 (60-kDa glycoprotein) receptors expressed on the tumor vasculature. Furthermore, SPARC (secreted protein, acidic and rich in cysteine) binds to albumin in the tumor interstitium and facilitates the uptake of albumin into tumors, providing the basis of targeted delivery by albumin nanoparticles [13–17]. Additionally, albumin itself plays a role as a dysopsonin that prevents the adsorption of various plasma proteins and protects macrophage recognition, leading to extended circulation time of nanoparticles [18,19]. In practice, the nab™ (nanoparticle albumin-bound) technology-based formulation, Abraxane®, has outperformed other existing formulations of paclitaxel, including Taxol®, by virtue of several significant advantages such as reduced toxicity, tolerated dose increase, and excellent tumor targetability. In this albumin nanoparticle structure, hydrophobic drugs play a significant role in assembling albumin by acting as physical cross-linkers.

Beta-carotene (BC) is a strongly red-orange-colored terpenoid that is synthesized biochemically from eight isoprene units in nature [20]. BC from many natural vegetable products, such as carrot, spinach, lettuce, and broccoli, is used as a safe natural dietary agent [21]. Some studies have reported the preventive effect of BC as a pro-vitamin by stimulating the immune system [22,23], showing an inverse relationship between BC uptake and risk of occurrence of estrogen receptor-negative [24,25] or –positive [26] breast cancers. BC has a high binding affinity to albumin, and its identical left-right symmetric structure has great potential for association of albumin molecules. On account of its high organic solubility it can be used as a physical cross-linker in the preparation of nab™ technology-based albumin nanoparticles in a similar manner to hydrophobic drugs.

In this study, a prototype of albumin nanoparticles consisting of naïve BSA, Ce6-BSA, and BC (Ce6-BSA-BC-NPs) was developed as a photodynamic therapy agent for the treatment of breast cancer in order to overcome the problems of poor solubility and tumor targetability. These albumin nanoparticles were fabricated using high-pressure homogenization based on nab™ technology and their physicochemical properties were examined. Also, the *in vitro* cytotoxicity and *in vivo* antitumor efficacy of Ce6-BSA-BC-NPs were examined in 4T1 cells (a triple-negative breast cancer cell line) and 4T1 cell-xenografted *nu/nu* mice after irradiation with 660-nm light (Fig. 1).

2. Materials and methods

2.1. Materials

Chlorin e6 (Ce6) was purchased from Frontier Scientific (Salt Lake City, UT, USA). Bovine serum albumin (BSA; 66.5 kDa and ~99%) and beta-carotene were from Sigma-Aldrich (St. Louis, MO, USA). 4T1 (ATCC® CRL-2539™) breast cancer cells were purchased from the Korean Cell Line Bank (Seoul, Korea). Dulbecco's modified Eagle's medium (DMEM), fetal bovine serum (FBS), and penicillin/streptomycin (P/S) were obtained from Corning (Corning, NY, USA). The LIVE/DEAD® viability/cytotoxicity kits for mammalian cells and singlet oxygen sensor green reagent (SOSG) were provided by Thermo Fisher Scientific (Rockford, IL, USA). The *in situ* cell death detection kit was obtained from Roche Diagnostics (Mannheim, Germany). All other reagents were supplied by Sigma-Aldrich unless otherwise specified.

2.2. Animals

BALB/c nu/nu mice (male, 6 weeks old) were purchased from Hanlim Experimental Animal Laboratory (Seoul, South Korea). Animals were cared for in accordance with the guidelines issued by the National Institutes of Health (NIH) according to the care and use of laboratory animals (NIH publication 80-23, revised in 1996). Mice were divided into groups corresponding to the treatment and provided with food and water under a 12-h light/dark cycle (lights on at 6 am). This study was approved by the Ethical Committee on Animal Experimentation at Sungkyunkwan University.

2.3. Preparation of Ce6-BSA conjugates

BSA was conjugated with Ce6 using a slight modification of previous methods [27,28]. In brief, aliquots of Ce6 (1 mmol), N-dicyclohexylcarbodiimide (DCC, 4 mmol), N- hydroxysuccinimide (NHS, 5 mmol) and triethylamine (TEA, 4 mmol) were dissolved in 10 ml dimethyl sulfoxide (DMSO, anhydrous) in a glass tube. The mixture was gently stirred and allowed to react in the dark at ambient temperature for 24 h. After removal of the precipitate, the Ce6-NHS produced was stored at −70 °C until use. Separately, different aliquots (1.5 and 4.5 ml) of Ce6-NHS (0.1 mmol) in DMSO, which correspond to feeding ratios of 20:1 and 60:1 (Ce6:BSA) respectively, were dropwise mixed with 50 ml BSA (0.0075 mmol) dissolved in 0.1 M sodium borate buffer (pH 8.5). The resulting suspension was continuously stirred at 450 rpm in the dark at room temperature for 24 h. Unreacted Ce6 and DMSO were removed using a dialysis membrane (MwCO: 10 kDa; amicon ultra, Millipore, Beverly, MA, USA) against 60% ethanol for 48 h and then against deionized water (DW) for 24 h. Finally, Ce6-BSA was concentrated in DW using a centrifugal concentrator (MwCO: 30 kDa, Amicon® Ultra, Millipore) and then lyophilized and stored at -20 °C for further experiments.

2.4. Characterization of Ce6-BSA conjugates

Ce6-BSA conjugates (feeding ratios of 20:1 or 60:1) were characterized by matrix-assisted laser desorption and ionization time of flight (MALDI-TOF) mass spectrometry (UltrafleXtreme, Bruker, Coventry, UK) and reversed-phase high-performance liquid chromatography (RP-HPLC) on a PLRP-S column (150 × 4.6 mm, 8 μm, Agilent Technologies, CA, USA) [28].

2.5. Preparation of Ce6-BSA-BC-NPs and BSA-BC-NPs

Ce6-BSA-BC-NPs and BSA-BC-NPs were prepared using a slight modification of nanoparticle albumin bound (nab™) technology [9,29,30]. In brief, aliquots of 40 mg BSA/10 mg Ce6-BSA (feeding ratio of 20:1) or 50 mg BSA were dissolved in 5 ml DW. Beta-carotene (1 mg) was dissolved in 100 μl of a 9:1 solution of chloroform and ethanol. These solutions consisting of aqueous and organic phases were gently mixed and homogenized using a WiseTis HG15D homogenizer (DAIHAN Scientific Co, Seoul, South Korea) at 18,000 rpm. The resulting solutions were passed through a high-pressure homogenizer (EmulsiFlex-B15 device, Avestin, Ottawa, Ontario, Canada) for nine cycles at 20,000 psi. The dispersions were rotary evaporated to remove chloroform at 40 °C for 15 min under reduced pressure. Finally, the NPs were centrifuged at 6000 rpm and the supernatants were lyophilized and stored at −20 °C until required.

2.6. Characterization of Ce6-BSA-BC-NPs and BSA-BC-NPs

The average particle sizes and zeta potentials of Ce6-BSA-BC-NPs and BSA-BC-NPs (each 1 mg/ml in DW) were measured using dynamic light scattering (DLS) (Zetasizer Nano ZS90, Malvern Instruments, Worcestershire, UK) with a 633-nm He-Ne laser beam and a fixed 90°

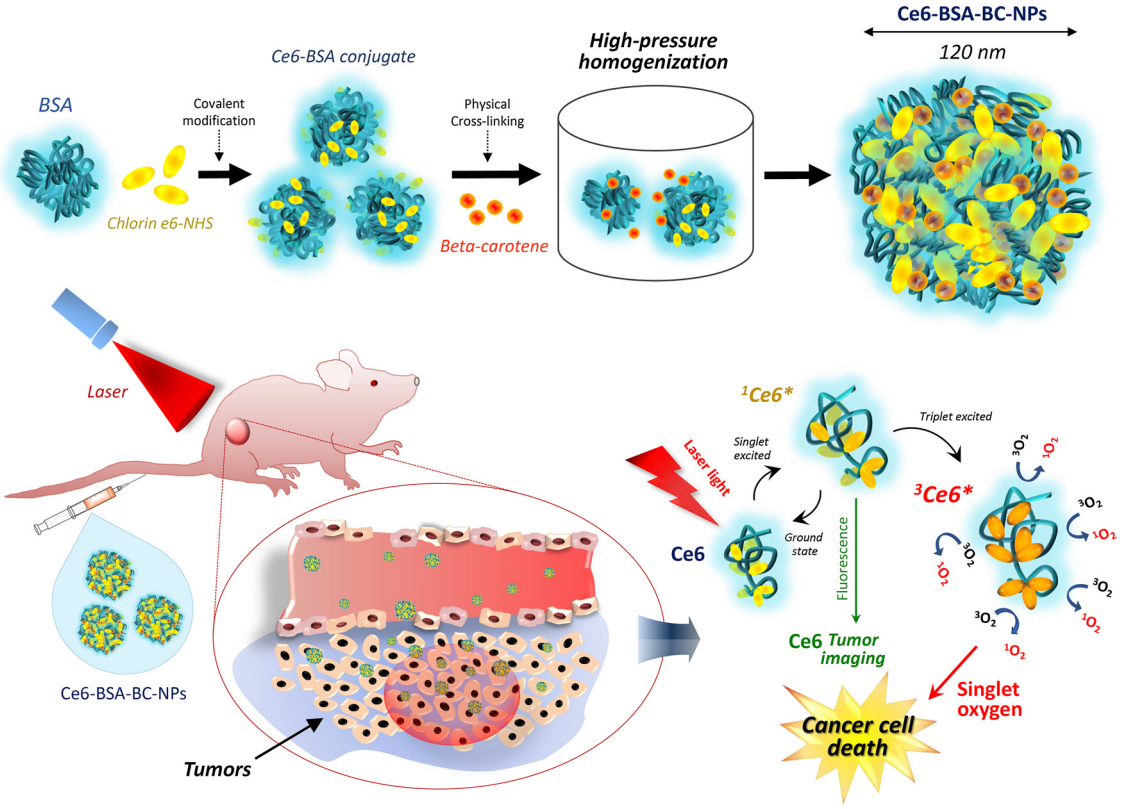

Fig. 1. Schematic illustration of preparation of Ce6-BSA-BC-NPs and photodynamic therapy in cancer tissues.

scattering angle. The surface morphology of the NPs was observed by transmission electron microscopy (TEM) with a model H-7600 microscope (Hitachi, Tokyo, Japan) and field-emission scanning electron microscopy (FE-SEM) using a LEO SUPRA 55 microscope (Carl Zeiss, Jena, Germany).

To investigate the physical stability of NPs, the particle sizes of Ce6-BSA-BC-NPs and BSA-BC-NPs (each 1 mg/ml in DW) were determined using the DLS method described above at room temperature over a 48-h period. The UV-VIS-NIR spectra of these samples were also recorded over 300–900 nm with a Synergy™ NEO microplate reader (Bio Tek, Winooski, VT, USA)

The encapsulation efficiency of BC in Ce6-BSA-BC-NPs or BSA-BC-NPs was determined using the following procedure. In brief, Ce6-BSA-BC-NPs (1 mg) dissolved in 0.1 ml DW were mixed with 0.9 ml acetone to extract BC and the resulting solution was thoroughly mixed and sonicated for 30 min. After centrifugation at 14,500 rpm for 20 min, the supernatant containing BC was withdrawn and acetone was completely removed by evaporation. The resulting BC diluted in *n*-hexane was quantified by UV spectrophotometry at 450 nm. The precipitate containing Ce6-BSA was reconstituted by a quantity of a 1:9 co-solvent of DMSO and DW and quantified by UV spectrophotometry at 660 nm.

2.7. Singlet oxygen generation profile

Singlet oxygen sensor green (SOSG) reagents were used as an indicator to detect singlet oxygen. In brief, free Ce6 (1 μg), Ce6-BSA, and Ce6-BSA-BC-NPs (each 1-μg equivalent as Ce6) were dissolved in 1 ml co-solvent (DMSO: DW = 1:9). SOSG was added to these solutions to a final concentration of 10 μM. BSA-BC-NPs and PBS with the same concentration of SOSG were prepared as positive and negative controls, respectively. The samples were irradiated with a 660-nm laser at a power of 10 mW/cm^2. Samples were withdrawn at 0, 10, 20, 30, 40 and 60 min for measurement of fluorescence intensity at excitation and emission wavelengths of 485 and 538 nm, respectively, using a TriStar^2 LB 942 Multimode Microplate Reader (Berthold Technologies GmbH & Co. KG, Württemberg, Germany). The effect of Ce6 concentration on singlet oxygen generation was observed using the same procedure.

2.8. Uptake of Ce6-BSA-BC-NPs into 4T1 cell spheroids

Three-dimensional culture of 4T1 cells to form spheroids was performed by a slight modification of previously described methods [9,10,31]. In brief, 200-μl aliquots of a hot agarose solution containing serum-free DMEM (2% w/v) with 1% penicillin/streptomycin were spread in each well of 12-well plates. The agarose solution was kept above 60 °C during the coating process to minimize agarose solidification and then cooled down to room temperature over 1 h. A 100-μl sample of cell suspension (10^6 cells) in DMEM containing 10% FBS) was seeded into each well and allowed to form spheroids over 3 days. Properly grown cell spheroids were treated with Ce6-BSA-BC-NPs (as a Ce6 equivalent of 10 μg/ml) and maintained for 24 h. After three washes with ice-cold PBS, the spheroids were transferred to glass bottom cell culture disks (diameter 20 mm, polystyrene) and observed by confocal laser scanning microscopy (CLSM) using the z stack image collection mode (20-μm step size, ~180-μm depth).

2.9. Cytotoxicity of Ce6-BSA-BC-NPs induced by laser irradiation in 4T1 cells

Three separate assays were conducted to evaluate the toxicity of Ce6-BSA-BC-NPs in conjunction with laser irradiation (660 nm): MTT, Live/Dead, and TUNEL (terminal deoxynucleotidyl transferase [TdT]-mediated dUTP nick end labeling) assays. First, the MTT assay was performed via slight modification of previously reported methods [28,32,33]. In brief, cells were seeded in 96-well plates at a density of 1×10^4 cells/well. After incubation for 24 h the cells were treated with different concentrations of free Ce6, Ce6-BSA, Ce6-BSA-BC-NPs, and BSA-BC-NPs The cells were further incubated for 2 h and then washed

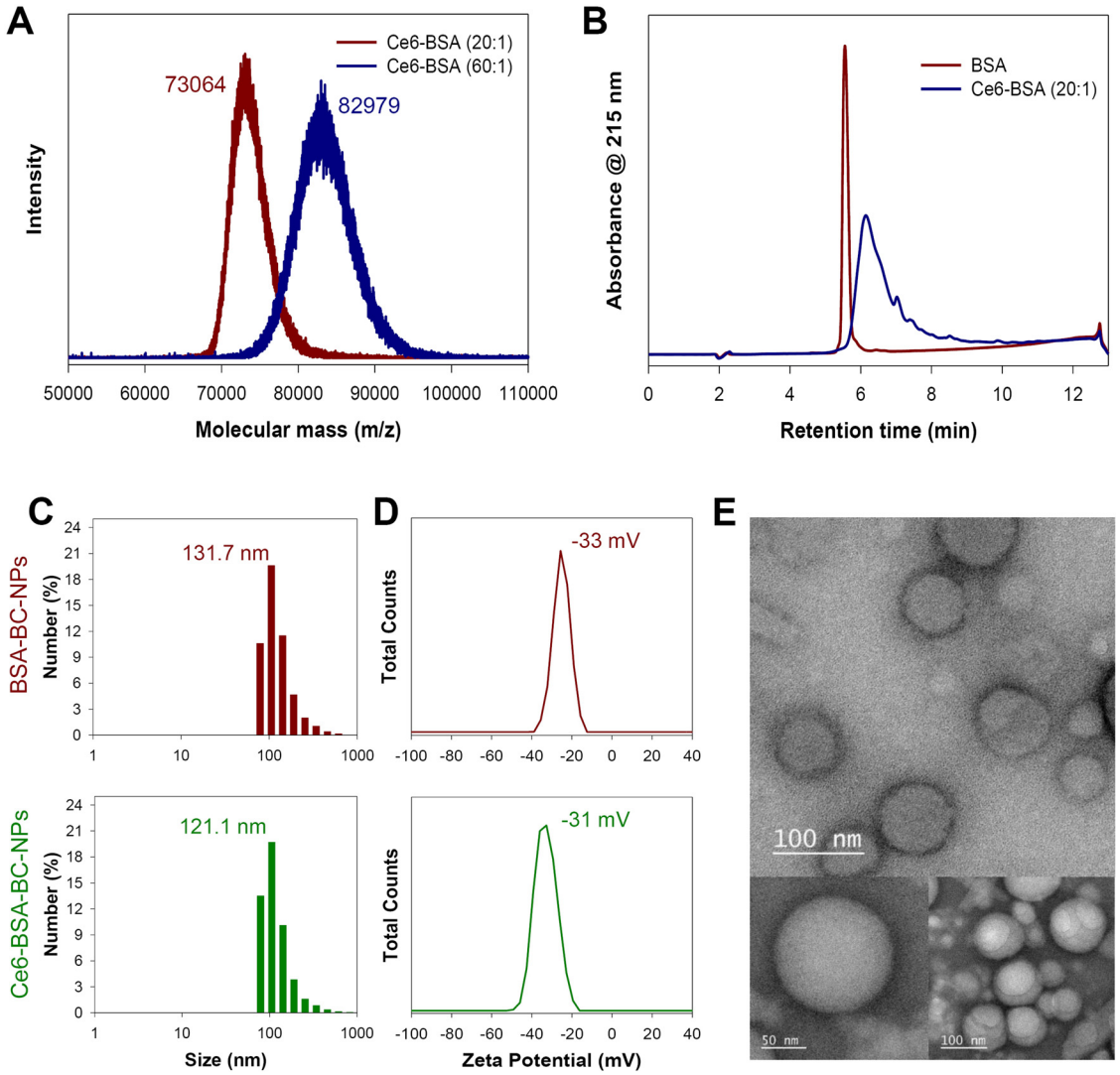

Fig. 2. (A) Matrix-assisted laser desorption and ionization time for flight (MALDI-TOF) mass spectra for Ce6-BSA at feed ratios of Ce6-NHS:BSA of 20:1 and 60:1. (B) Reverse-phase HPLC chromatograms for naïve BSA and Ce6-BSA (20:1). Histograms of particle size (C) and zeta potential (D) of BSA-BC-NPs and Ce6-BSA-BC-NPs, respectively. (E) TEM images of Ce6-BSA-BC-NPs.

three times, replenished with fresh media, and irradiated with 660-nm laser (10 mW/cm^2) for 30 min. After incubation for 24 h, the cytotoxicity (laser or without laser; photo toxicity or dark toxicity) was determined as the 50% inhibitory concentration (IC_{50}) using a 3-(4,5-dimethylthiazol-2-yl)-2,5-diphenyltetrazolium bromide (MTT)-based assay.

Live/Dead™ viability/cytotoxicity kits were used to visualize the death and viability of the 4T1 cells. Cells were seeded on 4-well glass slides (Lab-Tek® II Chamber Slide™ system, Sigma-Aldrich) at a density of 4×10^4 cells/well. After incubation for 12 h, the cells were treated with drug samples diluted in 1% DMEM (PBS, free Ce6, Ce6-BSA-BC-NPs, and BSA-BC-NP) and incubated for a further 2 h. The plates for each sample group were separated into laser-irradiated or non-irradiated and washed three times with PBS. The medium was replaced with fresh medium to remove any drug outside the cells prior to 660-nm irradiation for 30 min. After incubation for 2 h, live cells were stained green with Calcein-AM and dead cells were stained red with ethidium homodimer-1. The stained cells were observed by CLSM at excitation/emission wavelengths of 494/517 nm for Calcein-AM and 528/617 nm for ethidium homodimer-1.

The TUNEL assay was performed to identify apoptosis of 4T1 cells caused by the Ce6 moiety using an *in-situ* cell death detection kit (Fluorescein; Roche Diagnostics, Mannheim, Germany) according to the protocol described previously [9,28]. In brief, 1×10^5 cells were seeded onto glass slides in 6-well plates and treated with drugs using the same method as for the Live/Dead assay. After incubation for 2 h the medium was removed from each well by aspiration and 10% formalin was added to the cells for fixation over 1 h at room temperature. The cells were rinsed twice with ice-cold PBS and treated with 50 µl of TUNEL reagent in the dark at 37 °C for 1 h. The slides were then washed twice with PBS, dried, and stained with 4',6-diamidino-2-phenylindole (DAPI) solution containing nucleotides. The apoptotic cells were visualized using CLSM with a Meta LSM510 device (Carl Zeiss) with excitation/emission wavelengths of 450–490 and 520 nm, respectively.

2.10. *In vivo tumor targeting of Ce6-BSA-BC-NPs in 4T1-tumor-bearing mice*

The biodistribution and tumor targeting of Ce6-BSA-BC-NPs and free Ce6 were observed in mice bearing 4T1 tumors. Freshly harvested 4T1 cells (100-µl cell suspension containing 2×10^7 cells) were subcutaneously inoculated into each BALB/c *nu/nu* mouse. When the tumor volume reached ~100 mm^3, free Ce6 (2.5 mg/kg body) or Ce6-BSA-BC-NP (equivalent Ce6 of 2.5 mg/kg body) was injected into the

mice via the tail vein. The biodistribution was visualized as the fluorescence signal of the Ce6 moiety in both samples using a luminescence/fluorescence *in vivo* imaging system (SPECTRAL Lago X) at predetermined time points (1, 2, 4, 6, 8, and 24 h) post-injection.

2.11. Antitumor efficacy of Ce6-BSA-BC-NPs in 4T1-tumor-bearing mice

Mice were divided into four groups according to treatment: (i) PBS, (ii) free-Ce6, (iii) BSA-BC-NP, and (iv) Ce6-BSA-BC-NP. Every mouse in each group received intravenous injection of 100-μl aliquots of PBS or drug samples (as a Ce6 equivalent of 2.5 mg/kg body). The treated mice were irradiated twice with a laser (660 nm, 200 mW/cm^2) for 10 min at 4 h and 8 h post-injection, respectively. The tumor volumes and body weights of the treated mice were monitored every day for 2 weeks.

Separately, the histopathology of tumors was evaluated using a previously described procedure [23]. Tumors in each group were excised 24 h after treatment. The specimens were fixed with formalin, embedded in paraffin, sectioned, and stained with hematoxylin and eosin (H&E). The histopathology of the tumors in each group was compared under a light microscope.

2.12. Data analysis

Data are presented as the mean ± standard deviation (SD). Significant differences were determined using Student's t-tests. P values < 0.05 were considered statistically significant.

3. Results

3.1. Preparation and characterization of Ce6-BSA conjugate

Ce6-BSA conjugates were synthesized by conjugating activated chlorin e6 (Ce6-NHS) with the primary amines of BSA. The apparent molecular masses of Ce6-BSA conjugates (feed ratios of 20:1 or 60:1) were 73,064 and 82,979 *m/z*, respectively (Fig. 2A). This result indicated that approximately 11 and 28 Ce6 moieties were conjugated per BSA molecule for feed ratios of 20:1 or 60:1, respectively (Fig. 2A), based on the molecular weight of BSA (66.5 kDa). Increasing the degree of Ce6 attachment to BSA obviously increased its hydrophobicity, as evidenced by a delayed retention time and broader peak for Ce6-BSA (20:1) versus naïve BSA (Fig. 2B). However, Ce6-BSA (60:1) was even more hydrophobic and was not eluted in the applied HPLC condition due to high insolubility. Consequently, the Ce6-BSA (20:1) conjugate was chosen for further experiments and is hereafter referred to as Ce6-BSA.

3.2. Preparation and characterization of Ce6-BSA-BC-NPs and BSA-BC-NPs

Ce6-BSA-BC-NPs and BSA-BC-NPs were prepared using a high-pressure homogenizer based on nab™ technology. The size of Ce6-BSA-BC-NPs and BSA-BC-NPs was 121.1 ± 18.4 and 131.7 ± 17.5, respectively (Fig. 2C). The zeta potential of Ce6-BSA-BC-NPs and BSA-BC-NPs was -31 and −33 mV, respectively (Fig. 2D). Overall, there was little difference in size and zeta potential between the two particles. TEM results revealed that Ce6-BSA-BC-NPs were almost uniform and spherical (Fig. 2E). The encapsulation efficiency of Ce6 and BC into Ce6-BSA-BC-NPs was 96.8 ± 2.7 and 84.4 ± 3.8%, respectively. The stability of Ce6-BSA-BC-NPs and BSA-BC-NPs based on maintenance of particle size after fabrication was evaluated over 48 h. The particle size of Ce6-BSA-BC-NPs and BSA-BC-NPs changed slightly (from 112 to 165 nm and 135–180 nm, respectively) but was relatively well maintained (Fig. 3A). Ce6-BSA showed acceptable solubility and good dispersability in water (Fig. 3B), whereas Ce6, BC, and Ce6 plus BC showed very low water solubility (almost insoluble). Colloidal dispersion forms of Ce6-BSA-BC-NPs and BSA-BC-NPs after reconstitution were almost the same as before lyophilization, indicating good nanoparticle stability (Fig. 3C).

3.3. UV spectroscopic and singlet oxygen generation profiles

The absorption profiles of free Ce6, Ce6-BSA, BSA-BC-NPs, and Ce6-BSA-BC-NPs were investigated over the wavelength range between 300 and 900 nm. As shown in Fig. 4A, the sample groups including Ce6 (free Ce6, Ce6-BSA, and Ce6-BSA-BC-NPs) displayed significant peaks around 660 nm, which is a typical characteristic of chlorin e6. In contrast, BSA-BC-NPs had a very broad peak profile over 400–600 nm.

Separately, the fluorescence intensity caused by SOSG, which is a crucial parameter for the ability of singlet oxygen generation, was evaluated according to the sample group over 60 min. The SOSG fluorescence was proportional to both irradiation time (Fig. 4B) and Ce6 dose (not shown). In particular, increasing the irradiation time led to a significant increase in SOSG fluorescence in all groups containing Ce6, and their capacity for singlet oxygen generation appeared to be almost identical when adjusted for the equivalent amount of Ce6. Therefore, the capability of Ce6 to generate singlet oxygen in albumin nanoparticle groups was evidently retained after the nanoparticle fabrication process of organic phase exposure and high-pressure homogenization.

3.4. Uptake of Ce6-BSA-BC-NPs into 4T1 cell spheroids

Uptake of Ce6-BSA-BC-NPs into 4T1 cell spheroids was visualized by CLSM. Spheroids are considered to be an *in vitro* model system of tumors that mimics three-dimensional tumor tissues *in vivo*. 4T1 cell spheroids were treated with Ce6-BSA-BC-NPs for 24 h. The confocal spectroscopic images of 4T1 cell spheroids obtained from slices with a 20-μm step size showed clear red and green fluorescence, indicating that both BC and Ce6 were internalized into the spheroids (Fig. 5A). These results imply that Ce6-BSA-BC-NPs would be able to permeate into three-dimensional tumor tissues.

3.5. Cytotoxicity evaluations of Ce6-BSA-BC-NPs

As shown in Fig. 5B, Ce6-BSA-BC-NPs were cytotoxic to 4T1 cells after 660-nm laser irradiation (30 min, 10 mW/cm^2) over a wide Ce6 concentration range (62.5 ng/ml to 12 μg/ml). Except for BSA-BC-NPs, all groups (free Ce6, Ce6-BSA, and Ce6-BSA-BC-NPs) effectively killed 4T1 cells. The inhibitory concentrations (IC_{50}) values of free Ce6, Ce6-BSA, and Ce6-BSA-NPs were similar at 1.3, 1.4, and 1.6 μg/ml, respectively. As shown in Fig. 5B left, the groups including Ce6 moiety were shown to have slight toxicity to 4T1 cells at high concentrations (> 3 μg/ml). In the Live/Dead assays, almost all cells were killed after addition of free Ce6 and Ce6-BSA-BC-NPs followed by 660-nm laser irradiation, as visualized by red staining. Importantly, the cytotoxic effect of free Ce6 and Ce6-BSA-BC-NPs to 4T1 cells was only activated by the laser irradiation (Fig. 5C). In contrast, 4T1 cells treated with PBS or BSA-BC-NPs were evidently alive (visualized by green staining) regardless of laser irradiation. The apoptosis of 4T1 cells was visualized separately using TUNEL assay, and the fluorescence signals of BC and Ce6 in 4T1 cells were visualized by CLSM. As shown in Fig. 6, all 4T1 cells displayed signals of red and green fluorescence for BC and Ce6, respectively, regardless of laser irradiation, indicating internalization of Ce6-BSA-BC-NPs. In contrast, only 4T1 cells that were treated with Ce6-containing sample (free Ce6 and Ce6-BSA-BC-NPs groups) and irradiated by a 660-nm laser showed strong yellow fluorescence signals, indicating cell death caused by apoptosis due to singlet oxygen generation.

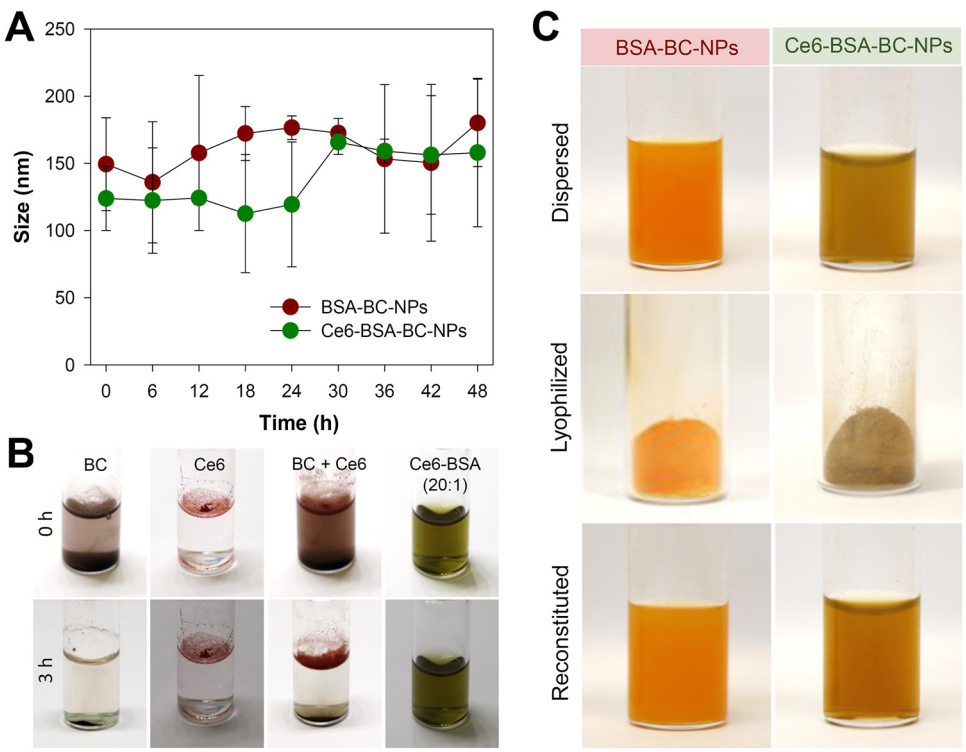

Fig. 3. (A) Physical stability of BSA-BC-NPs and Ce6-BSA-BC-NPs based on changes in size. (B) Photographs showing poor solubility of free BC, free Ce6, and free (BC + Ce6) in DW, and high solubility of Ce6-BSA (20:1) at 0 and 3 h (from left to right, respectively). (C) Photographs of solution (top), lyophilized powder (middle), and reconstituted suspension (bottom) of BSA-BC-NPs and Ce6-BSA-BC-NPs.

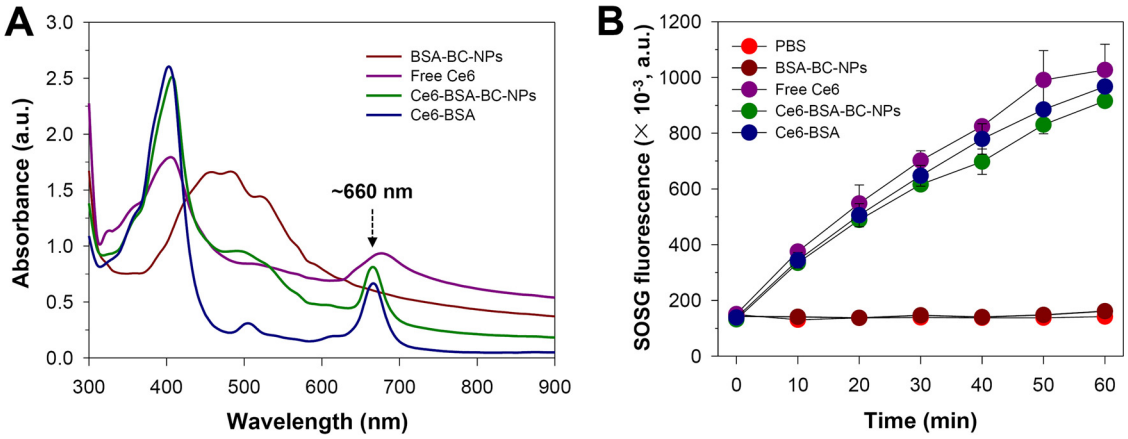

Fig. 4. (A) UV–vis-NIR absorption spectra and (B) singlet oxygen generation profile of Ce6-BSA-BC-NPs, BSA-BC-NPs, free Ce6, and Ce6-BSA (20:1).

3.6. In vivo tumor localization of Ce6-BSA-BC-NPs in 4T1 tumor-bearing mice

Free Ce6 did not appear to accumulate in specific tissue organs including tumors in 4T1 xenografted BALB/c nude mice but was spread over the whole body. In contrast, Ce6-BSA-BC-NPs were significantly localized in tumors of the mice. The tumor signal peaked at 4 h, persisted until ~8 h, and then faded out 24 h post-tail vein injection (Fig. 7).

3.7. Antitumor efficacy of Ce6-BSA-BC-NPs in 4T1 tumor-bearing mice

The photodynamic antitumor effects of Ce6-BSA-BC-NPs and control groups were evaluated in 4T1 tumor-bearing mice. The tumor volumes for each group of mice were measured over 14 days after treatment (Fig. 8A): the final tumor volumes for PBS, BSA-BC-NPs, free Ce6, and Ce6-BSA-BC-NPs groups were 687 ± 170, 607 ± 95, 487 ± 69, and 90 ± 39 mm^3, respectively. Remarkably, tumor growth in mice treated with Ce6-BSA-BC-NPs and laser irradiation was significantly suppressed and tumor size was 7-fold and 5-fold smaller than that of PBS and free Ce6 controls respectively (Fig. 8B and C). In terms of tumor morphology, the tumor surface of Ce6-BSA-BC-NP-treated mice became much darker than that of the other groups and transformed to almost black scabs on day 2 (Fig. 8B arrow). This indicated a higher level and faster manifestation of tumor cell death.

Tumor suppression based on cell density and color intensity was examined in the mice treated with Ce6-BSA-BC-NPs and control groups at 14 days after initiation of treatment. As shown in Fig. 8D, the photographic images of H&E-stained tumor sections from control groups displayed typical tumor overgrowth patterns, whereas the H&E image of sectioned tumor from mice of the Ce6-BSA-BC-NP group showed much weaker staining, indicating significant removal of compact tumor tissues due to cell death. The weight of mice in the four groups was maintained without significant change over 14 days, indicating that all mice were well cared for with no serious deleterious effects during the entire therapy period (Fig. 8E).

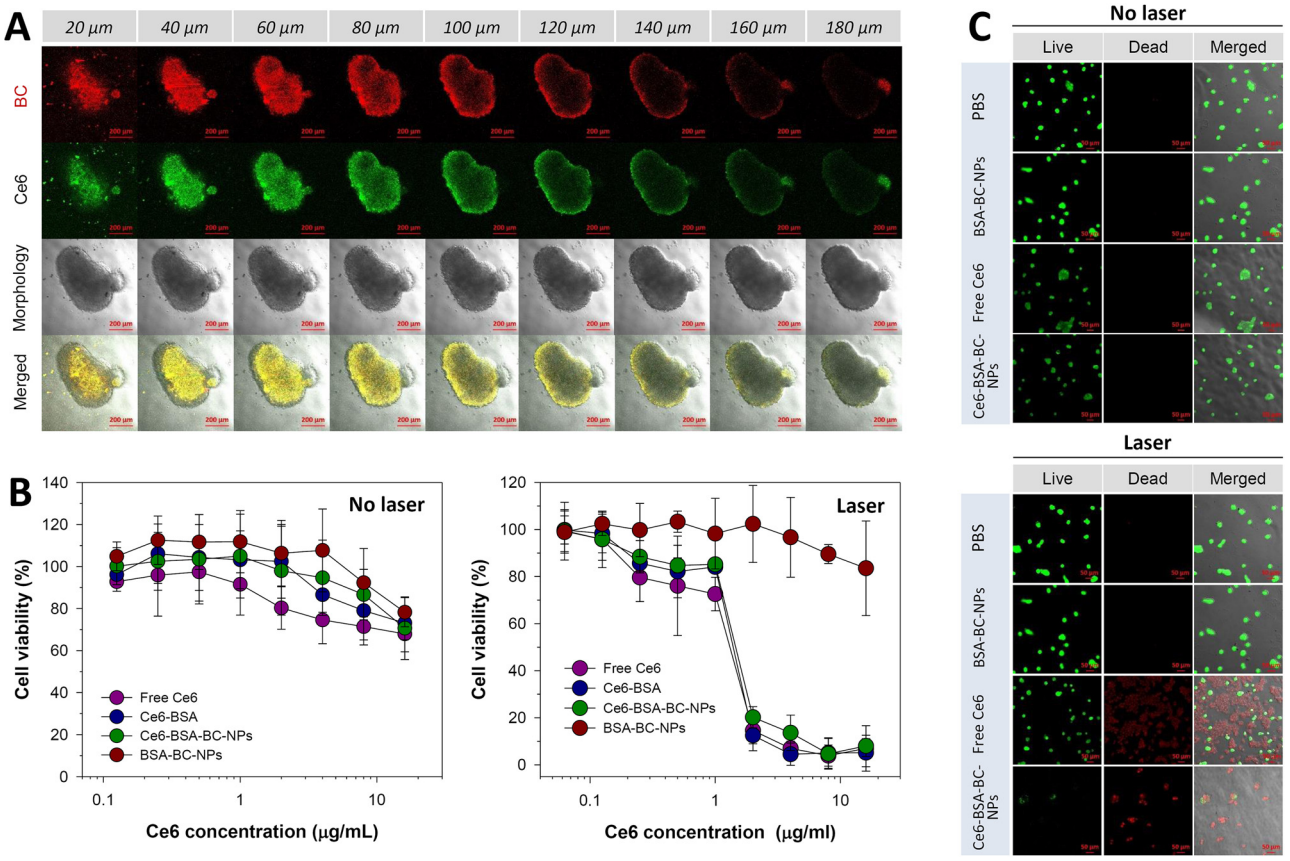

Fig. 5. (A) Permeability of Ce6-BSA-BC-NPs into 4T1 cell spheroids. Spheroids were treated with Ce6-BSA-BC-NPs (~10 μg/ml) and z-stack images of nine 20-μm slices were obtained. (B) Cytotoxicity of free Ce6, Ce6-BSA (20:1), Ce6-BSA-BC-NPs, and BSA-BC-NPs in 4T1 cells with (right) or without (left) laser irradiation (660 nm, 10 mW/cm^2 for 30 min) as evaluated by MTT assay. (C) Live/Dead assay of 4T1 cells incubated with PBS, BSA-BC-NPs, free Ce6, or Ce6-BSA-BC-NPs with and without irradiation with laser light (660 nm, 10 mW/cm^2 for 30 min).

4. Discussion

Photodynamic therapy (PDT) has attracted considerable attention as one of the most important therapeutic options due to its versatile applicability to cancer treatment [34]. The formalized protocol of PDT–local or systemic administration of photosensitizer (PS) followed by light irradiation–provides a convenient and efficient platform for cancer therapy. Despite many advantages over first-generation PSs (pophyrins), such as a long wavelength absorption range, deeper tissue penetration, fast tissue clearance, and higher extinction coefficients, the use of second-generation PSs (chlorins) has been restricted. In particular, chlorins are highly hydrophobic and aggregate easily in aqueous media, as observed in our study (Fig. 3B), which limits their practical applications [26]. Furthermore, second-generation PSs show poor tumor targetability with random body distribution (Fig. 7) [35]. Use of Ce6-conjugated BSA for targeted delivery of Ce6 and fabrication of albumin nanoparticles can overcome the problems of poor solubility and targetability, as described in our previous studies [13,29,31,36,37].

In the present study, chlorin e6 was conjugated with BSA via carboxyl group activation of Ce6 followed by modification with BSA. Ce6-BSA (feed ratio = 20:1) had 11 Ce6 moieties and was freely water-soluble, whereas Ce6-BSA (feed ratio = 60:1) had 28 Ce6 moieties and was insoluble in water (Figs. 2A and 3B). The increased solubility of Ce6-BSA (20:1) was essential for preparation of albumin nanoparticles and improved the *in vivo* availability of Ce6 for photodynamic therapy.

Despite the excellent targetability of naïve albumin, Ce6-modified albumin might lose its inherent gp60 binding property due to the high level of Ce6 modification on its surface. Thus, Ce6-BSA-BC-NPs were formulated using the minimum amount of Ce6 required to maintain acceptable targetability to tumors. Moreover, the increased use of modified albumin vs. naïve albumin might result in a reduced ability for albumin association during high-pressure homogenization [31]. For these reasons, only 20% Ce6-BSA (20:1; 80% naïve BSA) was used to prepare the albumin nanoparticles (Ce6-BSA-BC-NPs).

When preparing albumin nanoparticles using nab™ technology, hydrophobic compounds are inevitably required for cross-linking of albumin molecules through physical attachment to the hydrophobic pocket in albumin [11]. In general, hydrophobic chemotherapeutics (soluble in chloroform) such as paclitaxel, docetaxel, or doxorubicin, have performed dual functions as anticancer drugs and physical cross-linkers. In our study we did not use highly toxic chemotherapeutics but instead used the natural product beta-carotene as a physical cross-linker. As shown in Fig. 3B, BC was sufficiently hydrophobic to bridge albumin molecules via high-press homogenization, producing ~120-nm spherical albumin nanoparticles. The resulting albumin nanoparticles (Ce6-BSA-BC-NPs) were stably maintained at ambient temperature over 48 h without significant changes in particle size, which was very similar to the size of commercially available Abraxane® (~130 nm). The Vis-UV-NIR spectrum displayed the typical peak (~660 nm) of Ce6. Moreover, Ce6-BSA-BC-NPs were highly dispersible, well lyophilized, and easily reconstituted, crucial characteristics for manufacture.

The singlet oxygen sensor green reagent is well-documented to specifically react with $^1O_2$ [38]. In the presence of singlet oxygen, this indicator exhibits green fluorescence at excitation/emission maximal wavelengths of ~504/525 nm, respectively, and the intensity of the produced fluorescence signal correlates well with $^1O_2$ concentration without interference from other reactive oxygen species [39]. Our Ce6-

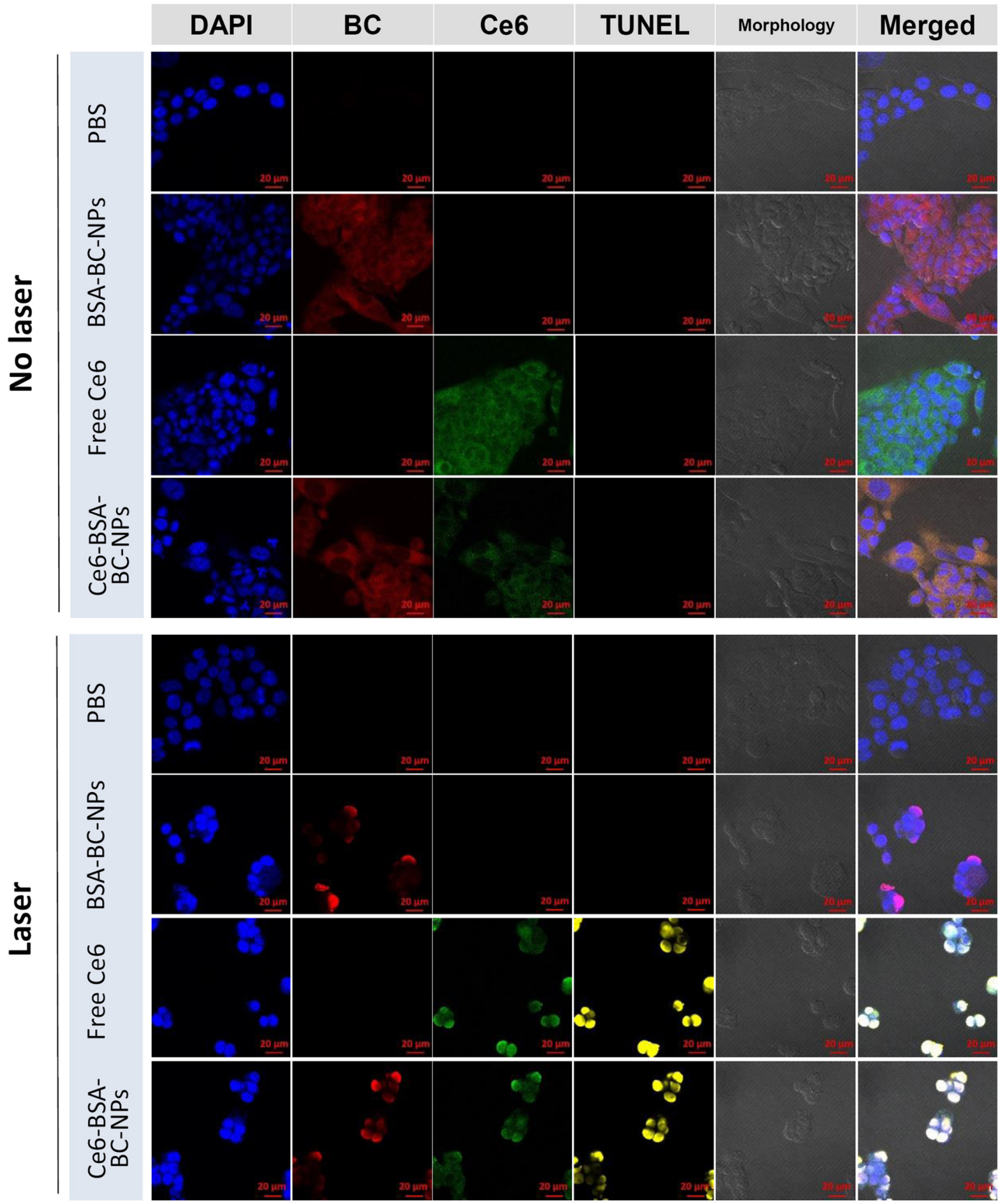

Fig. 6. Cytotoxicity evaluation based on TUNEL assay of 4T1 cells incubated with PBS, BSA-BC-NPs, free Ce6, or Ce6-BSA-BC-NPs with and without irradiation with laser light (660 nm, 10 mW/cm^2 for 30 min).

BSA-BC-NPs were found to have almost same singlet oxygen-generating activity as free Ce6 and Ce6-BSA at normalized concentrations of Ce6. This indicated that the Ce6 activity of Ce6-BSA-BC-NPs was well preserved during the series of harsh manufacturing steps including conjugation, high-pressure homogenization, evaporation, free-drying, and reconstitution. However, fractions of singlet oxygen that are close to the area of its production have limited use in destroying cancer cells because of their high sensitivity and short half-life when light irradiated [40,41]. In this respect, albumin is considered a good nanomaterial for carrying and localizing Ce6 at a high concentration in specific tumor sites where laser light is focused via passive and active accumulation (Fig. 7).

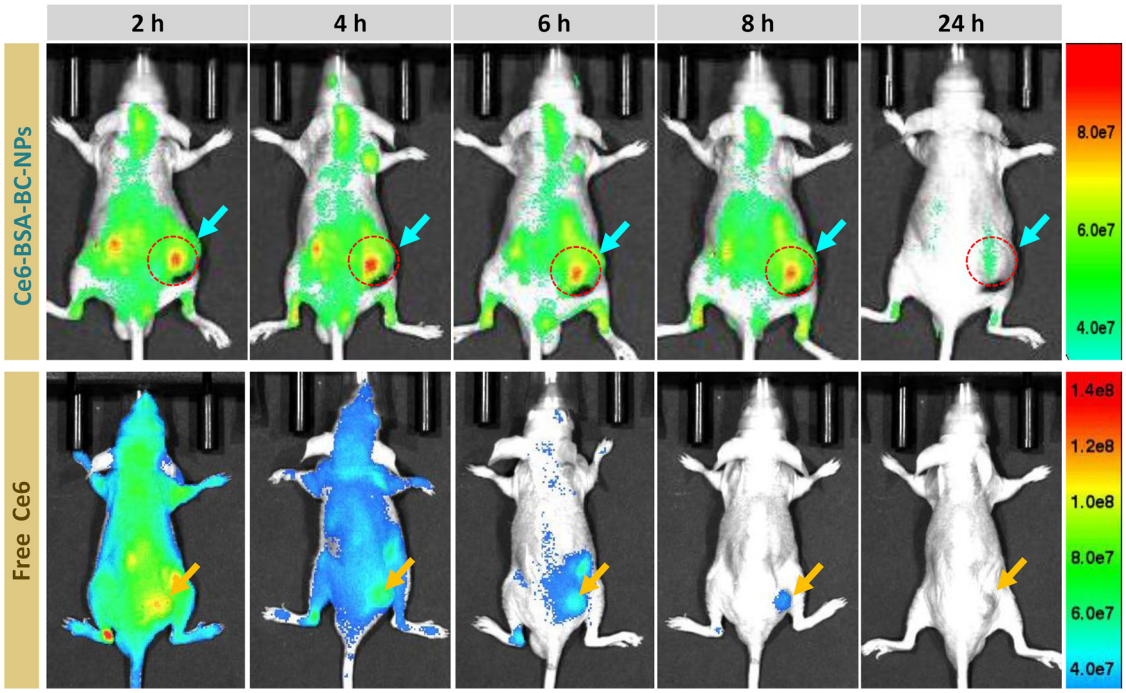

Fig. 7. *In vivo* monitoring of tumor targeting of Ce6-BSA-BC-NPs and free Ce6 in 4T1 tumor-bearing mice.

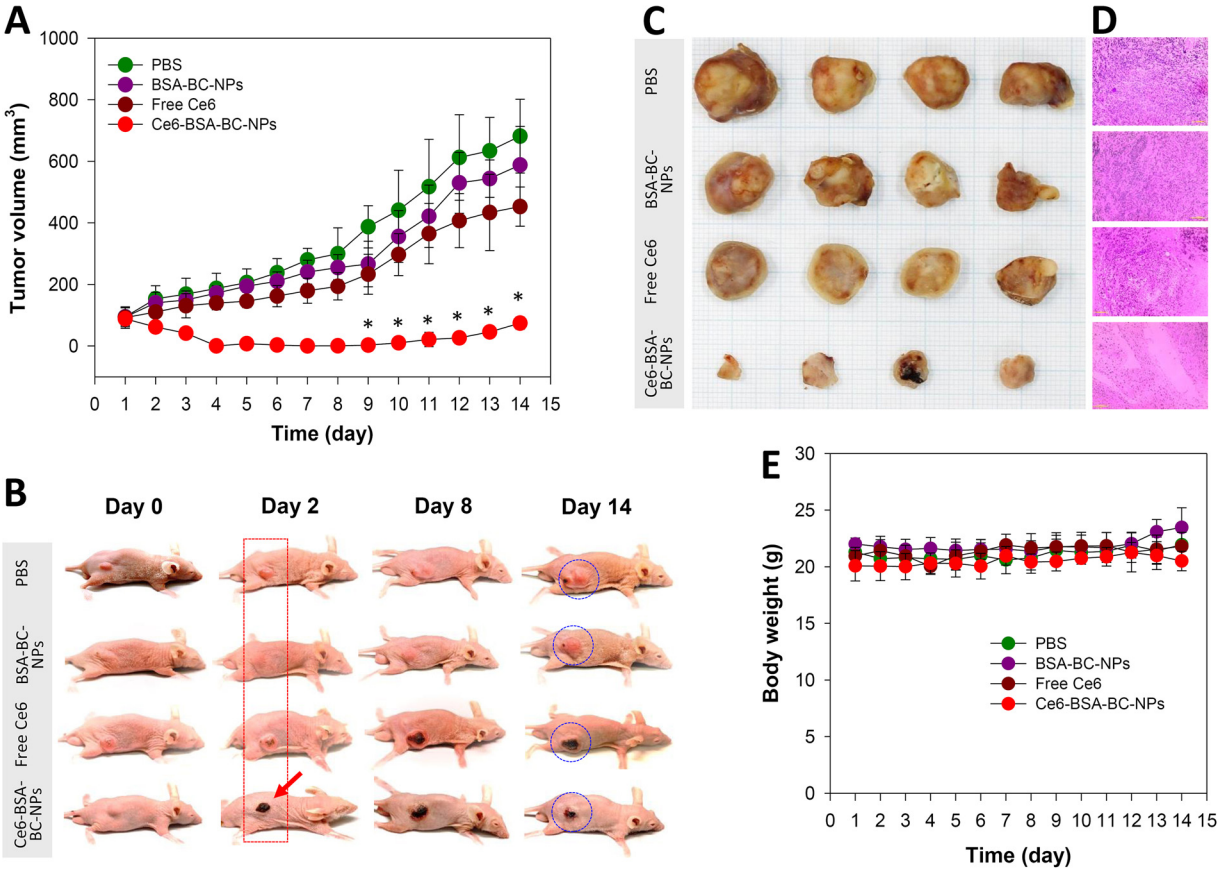

Fig. 8. *In vivo* antitumor efficacy induced by Ce6-BSA-BC-NPs and free Ce6. (A) Profiles for tumor growth of 4T1 tumor-bearing mice treated with PBS, BC-BSA-NPs (equivalent amount of BC amount as in Ce6-BSA-BC-NPs), free Ce6 (2.5 mg/kg), and Ce6-BSA-BC-NPs (2.5 mg/kg Ce6). *$P < 0.001$ over all other groups. (B) Representative photographs of 4T1 tumor-bearing mice over 14 days after treatment. (C) Photographs of tumors harvested from the different treatment groups. (D) H &E–stained tumor tissues of each group at 24 h post-treatment. (E) Body weight change of 4T1 tumor-bearing mice in the different treatment groups over 14 days after treatment.

Regarding *in vitro* cytotoxicity, cell viability Ce6-BSA-BC-NPs were shown to penetrate 4T1 cells or spheroids (mimicking 3D solid tumors) and exhibited almost equivalent cytotoxicity to that of free Ce6 or Ce6-BSA when irradiated at 660 nm (Figs. 5C and 6). In addition, the on-off pattern of Ce6-BSA-BC-NPs in response to 660-nm light irradiation was clear in terms of cell-killing activity. The resulting phototoxicity depended on the presence of both Ce6 and appropriate laser irradiation, unlike slight or negligible dark toxicity (Fig. 5B). This suggests that targeted Ce6-BSA-BC-NPs and localized laser would minimize the non-specific toxicity to other normal tissue sites around tumors.

With regard to *in vivo* efficacy, the interval between administration of PS and light exposure was a key factor for PDT efficacy [3]. Previous studies have used widely different dosing intervals, for example, tens of minutes to a few days [42,43], which are usually determined by the formulation or tumor physiology. However, differences in the time interval influence the mechanisms by which tumor cells are killed and result in different consequences of therapy [44]. In our study, the timing of light irradiation was determined as the time point when the Ce6 signal reached a peak. To achieve dual efficacy, the light (660 nm) was illuminated onto the tumor sites of 4T1 tumor-bearing mice at 4 h and 8 h (200 mW/cm^2 for each 10 min) because the peak fluorescence signal from Ce6-BSA-BC-NPs maintained for 4–8 h after the injection. Under this optimized condition, Ce6-BSA-BC-NPs suppressed the 4T1 tumors much more effectively than free Ce6 (tumor volume 90 ± 39 and 487 ± 69 mm^3, respectively; Fig. 8A).

In agreement with the previous results [1,45,46], apoptosis seemed to be mainly responsible for tumor cell death caused by Ce6-BSA-BC-NPs as shown in the TUNEL results (Fig. 6), among modes of cell death (necrosis, apoptosis, or autophagy) induced by PDT. However, the mechanism of cell death also depends on the concentration of activated Ce6; a high level of activated Ce6 often triggers necrotic cell death whereas a low level tends to induce apoptosis and autophagy [1,5,47]. Due to improved tumor targetability and long circulation, the activated Ce6 (from Ce6-BSA-BC-NP) seemed to accumulate highly in the tumors, causing black scabs on the surface of these tumors two days after the treatment. On the contrary, few black scabs were observed in mice treated with free Ce6 (Fig. 8B). Additionally, it was observed that another mice group treated with Ce6-BSA-BC-NPs and low laser intensity (data not shown) did show few dark site (scab), showing moderate tumor ablation, which strengthens the hypothesis of apoptotic pathway in terms of cell death. After the initial period, the tumors appeared to be gradually suppressed over two weeks through apoptosis induced by the low level of activated Ce6 in both mice group treated with free Ce6 and Ce6-BSA-BC-NPs.

To our best knowledge, other PDT-based albumin NP platforms involve in the fabrication (e.g., self-assembly, desolvation or nano-precipitation) followed by a permanent covalent cross-linking step using carbodiimide derivatives (EDC) or glutaraldehyde to stabilize the resulting NP structures [32,33,48,49]. This cross-linking firmly maintains the original size of the NPs even in plasma for long. In contrast, our Ce6-BSA-BC-NPs are prepared using the Nab™ method that assembles albumin molecules via physical cross-linking, not covalently. In this respect, it is of great importance that Abraxane® quickly dissociate into smaller albumin adducts (~10 nm) in plasma, despite their original sizes of ~130 nm [50–53]. This common phenomenon of *in vivo* breakdown of the Nab™-based albumin NPs (but still having antitumor moieties) enhances both extravasation-based 'passive' targeting and gp60 receptor-based 'active' targeting [11,13,54]. Many articles claim that relatively large nanoparticles (~100-200 nm) do not practically accumulate in the tumors much less than expected by the enhanced permeability and retention (EPR) effect, despite large pores of tumor vessels [52,55,56]. We believe this would be another practical advantage of our Ce6-BSA-BC-NPs for better clinical efficacy.

5. Conclusion

A prototype of albumin nanoparticles consisting of BSA, Ce6-BSA, and beta-carotene was developed using a modification of nab™ technology. These albumin nanoparticles (Ce6-BSA-BC-NPs) did not include any toxic chemotherapeutics but instead contained naturally safe beta-carotene and Ce6 that was activated only when irradiated with 660 nm laser light. The Ce6-BSA-BC-NPs were ~120 nm in size and spherical, and showed good physicochemical stability as well as significant cytotoxicity as evaluated by MTT, Live/Dead, and TUNEL assays. Ce6-BSA-BC-NPs displayed a superior tumor suppression effect when irradiated by 660 nm light compared with free Ce6. This improved antitumor efficacy seemed to be due to the targetability of albumin nanoparticles. Our findings demonstrate that Ce6-BSA-BC-NPs might be a promising platform for cancer treatment in the near future.

Acknowledgment

This research was supported by a grant (16173MFDS542) from the Ministry of Food and Drug Safety in 2018.

References

[1] S.S. Lucky, K.C. Soo, Y. Zhang, Nanoparticles in photodynamic therapy, Chem. Rev. 115 (2015) 1990–2042.
[2] H.S. Hwang, H. Shin, J. Han, K. Na, Combination of photodynamic therapy (PDT) and anti-tumor immunity in cancer therapy, J. Pharm. Investig. 48 (2018) 143–151.
[3] D.E. Dolmans, D. Fukumura, R.K. Jain, Photodynamic therapy for cancer, Nat. Rev. Cancer 3 (2003) 380.
[4] P. Mroz, A. Yaroslavsky, G.B. Kharkwal, M.R. Hamblin, Cell death pathways in photodynamic therapy of cancer, Cancers (Basel) 3 (2011) 2516–2539.
[5] E. Buytaert, M. Dewaele, P. Agostinis, Molecular effectors of multiple cell death pathways initiated by photodynamic therapy, Biochim. Biophys. Acta. 1776 (2007) 86–107.
[6] G.M.F. Calixto, J. Bernegossi, L.M. de Freitas, C.R. Fontana, M. Chorilli, Nanotechnology-based drug delivery systems for photodynamic therapy of cancer: a review, Molecules 21 (2016) 342.
[7] S. ho Hong, Y. Choi, Mesoporous silica-based nanoplatforms for the delivery of photodynamic therapy agents, J. Pharm. Investig. 48 (2018) 3–17.
[8] J.P. Celli, B.Q. Spring, I. Rizvi, C.L. Evans, K.S. Samkoe, S. Verma, B.W. Pogue, T. Hasan, Imaging and photodynamic therapy: mechanisms, monitoring, and optimization, Chem. Rev. 110 (2010) 2795–2838.
[9] B. Kim, B. Seo, S. Park, C. Lee, J.O. Kim, K.T. Oh, E.S. Lee, H.-G. Choi, Y.S. Youn, Albumin nanoparticles with synergistic antitumor efficacy against metastatic lung cancers, Colloids Surf. B 158 (2017) 157–166.
[10] H.J. Byeon, C. Lee, S. Lee, E.S. Lee, Y.W. Choi, H.-G. Choi, E.-S. Park, K.C. Lee, Y.S. Youn, Doxorubicin-bound albumin nanoparticles containing a TRAIL protein for targeted treatment of colon cancer, Pharm. Res. 33 (2016) 615–626.
[11] F. Kratz, Albumin as a drug carrier: design of prodrugs, drug conjugates and nanoparticles, J. Control. Release 132 (2008) 171–183.
[12] H. Maeda, J. Wu, T. Sawa, Y. Matsumura, K. Hori, Tumor vascular permeability and the EPR effect in macromolecular therapeutics: a review, J. Control. Release 65 (2000) 271–284.
[13] E.S. Lee, Y.S. Youn, Albumin-based potential drugs: focus on half-life extension and nanoparticle preparation, J. Pharm. Investig. 46 (2016) 305–315.
[14] T. Lin, P. Zhao, Y. Jiang, Y. Tang, H. Jin, Z. Pan, H. He, V.C. Yang, Y. Huang, Blood–brain-barrier-penetrating albumin nanoparticles for biomimetic drug delivery via albumin-binding protein pathways for antiglioma therapy, ACS Nano 10 (2016) 9999–10012.
[15] H. Sage, C. Johnson, P. Bornstein, Characterization of a novel serum albumin-binding glycoprotein secreted by endothelial cells in culture, J. Chem. Biol. 259 (1984) 3993–4007.
[16] M.J. Hawkins, P. Soon-Shiong, N. Desai, Protein nanoparticles as drug carriers in clinical medicine, Adv. Drug Del. Rev. 60 (2008) 876–885.
[17] C. Tiruppathi, W. Song, M. Bergenfeldt, P. Sass, A.B. Malik, Gp60 activation mediates albumin transcytosis in endothelial cells by tyrosine kinase-dependent pathway, J. Chem Biol. 272 (1997) 25968–25975.
[18] K.-i. Ogawara, K. Furumoto, S. Nagayama, K. Minato, K. Higaki, T. Kai, T. Kimura, Pre-coating with serum albumin reduces receptor-mediated hepatic disposition of polystyrene nanosphere: implications for rational design of nanoparticles, J. Control. Release 100 (2004) 451–455.
[19] Q. Peng, S. Zhang, Q. Yang, T. Zhang, X.-Q. Wei, L. Jiang, C.-L. Zhang, Q.-M. Chen, Z.-R. Zhang, Y.-F. Lin, Preformed albumin corona, a protective coating for nanoparticles based drug delivery system, Biomaterials 34 (2013) 8521–8530.
[20] B. Tan, D.N. Soderstrom, Qualitative aspects of UV-vis spectrophotometry of beta-carotene and lycopene, J. Chem. Educ. 66 (1989) 258.
[21] K.A. Steinmetz, J.D. Potter, Vegetables, fruit, and cancer. II. Mechanisms, Cancer Causes Control 2 (1991) 427–442.
[22] B.P. Chew, J.S. Park, Carotenoid action on the immune response, J. Nutr. 134

(2004) 257S–261S.
[23] C.B. Stephensen, Vitamin a, infection, and immune function, Annu. Rev. Nutr. 21 (2001) 167–192.
[24] X. Zhang, D. Spiegelman, L. Baglietto, L. Bernstein, D.A. Boggs, P.A. Van Den Brandt, J.E. Buring, S.M. Gapstur, G.G. Giles, E. Giovannucci, Carotenoid intakes and risk of breast cancer defined by estrogen receptor and progesterone receptor status: a pooled analysis of 18 prospective cohort studies, Am. J. Clin. Nutr. 95 (2012) 713–725.
[25] M.F. Bakker, P.H. Peeters, V.M. Klaasen, H.B. Bueno-de-Mesquita, E.H. Jansen, M.M. Ros, N. Travier, A. Olsen, A. Tjønneland, K. Overvad, Plasma carotenoids, vitamin C, tocopherols, and retinol and the risk of breast cancer in the European prospective investigation into cancer and nutrition cohort, 2, Am, J. Clin. Nutr. 103 (2016) 454–464.
[26] Y. Cui, J.M. Shikany, S. Liu, Y. Shagufta, T.E. Rohan, Selected antioxidants and risk of hormone receptor–defined invasive breast cancers among postmenopausal women in the women's health initiative observational study, Am. J. Clin. Nutr. 87 (2008) 1009–1018.
[27] S.Y. Park, K.T. Oh, Y.T. Oh, N.M. Oh, Y.S. Youn, E.S. Lee, An artificial photosensitizer drug network for mitochondria-selective photodynamic therapy, Chem. Commun. (Camb.) 48 (2012) 2522–2524.
[28] C. Lee, B. Kim, S. Lee, T.H. Kim, J.O. Kim, E.S. Lee, K.T. Oh, H.-G. Choi, S.D. Yoo, Y.S. Youn, Doxorubicin and paclitaxel co-bound lactosylated albumin nanoparticles having targetability to hepatocellular carcinoma, Colloids Surf. B 152 (2017) 183–191.
[29] T.H. Kim, H.H. Jiang, Y.S. Youn, C.W. Park, K.K. Tak, S. Lee, H. Kim, S. Jon, X. Chen, K.C. Lee, Preparation and characterization of water-soluble albumin-bound curcumin nanoparticles with improved antitumor activity, Int. J. Pharm. 403 (2011) 285–291.
[30] N.P. Desai, C. Tao, A. Yang, L. Louie, T. Zheng, Z. Yao, P. Soon-Shiong, S. Magdassi, 1999. Protein stabilized pharmacologically active agents, methods for the preparation thereof and methods for the use thereof, Google Patents.
[31] H.J. Byeon, S. Lee, S.Y. Min, E.S. Lee, B.S. Shin, H.-G. Choi, Y.S. Youn, Doxorubicin-loaded nanoparticles consisted of cationic-and mannose-modified-albumins for dual-targeting in brain tumors, J. Control. Release 225 (2016) 301–313.
[32] H. Jeong, M. Huh, S.J. Lee, H. Koo, I.C. Kwon, S.Y. Jeong, K. Kim, Photosensitizer-conjugated human serum albumin nanoparticles for effective photodynamic therapy, Theranostics 1 (2011) 230.
[33] Q. Chen, X. Wang, C. Wang, L. Feng, Y. Li, Z. Liu, Drug-induced self-assembly of modified albumins as nano-theranostics for tumor-targeted combination therapy, ACS Nano 9 (2015) 5223–5233.
[34] M. Triesscheijn, P. Baas, J.H. Schellens, F.A. Stewart, Photodynamic therapy in oncology, Oncologist 11 (2006) 1034–1044.
[35] E. Paszko, C. Ehrhardt, M.O. Senge, D.P. Kelleher, J.V. Reynolds, Nanodrug applications in photodynamic therapy, Photodiagnosis Photodyn. Ther. 8 (2011) 14–29.
[36] S. Bae, K. Ma, T.H. Kim, E.S. Lee, K.T. Oh, E.-S. Park, K.C. Lee, Y.S. Youn, Doxorubicin-loaded human serum albumin nanoparticles surface-modified with TNF-related apoptosis-inducing ligand and transferrin for targeting multiple tumor types, Biomaterials 33 (2012) 1536–1546.
[37] H.J. Byeon, S.Y. Min, I. Kim, E.S. Lee, K.T. Oh, B.S. Shin, K.C. Lee, Y.S. Youn, Human serum albumin-TRAIL conjugate for the treatment of rheumatoid arthritis, Bioconjug. Chem. 25 (2014) 2212–2221.
[38] X. Ragàs, A. Jiménez-Banzo, D. Sánchez-García, X. Batllori, S. Nonell, singlet oxygen photosensitisation by the fluorescent probe singlet oxygen sensor Green®, Chem. Commun. (Camb.) (2009) 2920–2922.
[39] S. Kim, M. Fujitsuka, T. Majima, Photochemistry of singlet oxygen sensor green, J. Phys. Chem. B 117 (2013) 13985–13992.
[40] D.K. Chatterjee, L.S. Fong, Y. Zhang, Nanoparticles in photodynamic therapy: an emerging paradigm, Adv. Drug Del. Rev. 60 (2008) 1627–1637.
[41] C.A. Robertson, D.H. Evans, H. Abrahamse, Photodynamic therapy (PDT): a short review on cellular mechanisms and cancer research applications for PDT, J. Photochem. Photobiol. B 96 (2009) 1–8.
[42] T.J. Dougherty, An update on photodynamic therapy applications, J. Clin. Laser Med. Surg. 20 (2002) 3–7.
[43] P. Cramers, M. Ruevekamp, H. Oppelaar, O. Dalesio, P. Baas, F. Stewart, Foscan® uptake and tissue distribution in relation to photodynamic efficacy, Br. J. Cancer 88 (2003) 283.
[44] B.W. Pogue, J.A. O'hara, E. Demidenko, C.M. Wilmot, I.A. Goodwin, B. Chen, H.M. Swartz, T. Hasan, Photodynamic therapy with verteporfin in the radiation-induced fibrosarcoma-1 tumor causes enhanced radiation sensitivity, Cancer Res. 63 (2003) 1025–1033.
[45] H. Guo, H. Qian, N.M. Idris, Y. Zhang, Singlet oxygen-induced apoptosis of cancer cells using upconversion fluorescent nanoparticles as a carrier of photosensitizer, Nanomedicine 6 (2010) 486–495.
[46] M. Wawrzyńska, W. Kałas, D. Biały, E. Zioło, J. Arkowski, W. Mazurek, L. Strządała, In vitro photodynamic therapy with chlorin e6 leads to apoptosis of human vascular smooth muscle cells, Arch. Immunol. Ther. Exp. (Warsz.) 58 (2010) 67–75.
[47] F.H. van Duijnhoven, R.I. Aalbers, J.P. Rovers, O.T. Terpstra, P.J. Kuppen, The immunological consequences of photodynamic treatment of cancer, a literature review, Immunobiology 207 (2003) 105–113.
[48] I. Shton, V. Sarnatskaya, I. Prokopenko, N. Gamaleia, Chlorin e6 combined with albumin nanoparticles as a potential composite photosensitizer for photodynamic therapy of tumors, Exp. Oncol. (2015) 250–254.
[49] A.M. Molina, M. Morales-Cruz, M. Benítez, K. Berríos, C.M. Figueroa, K. Griebenow, Redox-sensitive cross-linking enhances albumin nanoparticle function as delivery system for photodynamic cancer therapy, J. Nanomed. Nanotechnol. 6 (2016).
[50] V. Narayanan, C.D. Weekes, Nanoparticle albumin-bound (nab)-paclitaxel for the treatment of pancreas ductal adenocarcinoma, Gastrointest. Cancer 5 (2015) 11–19.
[51] N. Chen, C. Brachmann, X. Liu, D.W. Pierce, J. Dey, W.S. Kerwin, Y. Li, S. Zhou, S. Hou, M. Carleton, Albumin-bound nanoparticle (nab) paclitaxel exhibits enhanced paclitaxel tissue distribution and tumor penetration, Cancer Chemother. Pharmacol. 76 (2015) 699–712.
[52] J.W. Nichols, Y.H. Bae, EPR: evidence and fallacy, J. Control. Release 190 (2014) 451–464.
[53] D.A. Yardley, nab-Paclitaxel mechanisms of action and delivery, J. Control. Release 170 (2013) 365–372.
[54] A.O. Elzoghby, W.M. Samy, N.A. Elgindy, Albumin-based nanoparticles as potential controlled release drug delivery systems, J. Control. Release 157 (2012) 168–182.
[55] H. Cabral, Y. Matsumoto, K. Mizuno, Q. Chen, M. Murakami, M. Kimura, Y. Terada, M. Kano, K. Miyazono, M. Uesaka, Accumulation of sub-100 nm polymeric micelles in poorly permeable tumours depends on size, Nat. Nanotechnol. 6 (2011) 815.
[56] Y.H. Bae, K. Park, Targeted drug delivery to tumors: myths, reality and possibility, J Control. Release 153 (2011) 198.